

3D-Printed PLA Filaments Reinforced with Nanofibrillated Cellulose

Matea Perić^{1,*}, Robert Putz¹ and Christian Paulik²

¹Wood K Plus-Competence Center for Wood Composites & Wood Chemistry, Kompetenzzentrum Holz GmbH, Linz, A-4040, Austria

²Institute for Chemical Technology of Organic Materials, Johannes Kepler University Linz, Linz, 4040, Austria

*Corresponding Author: Matea Perić. Email: m.peric@wood-kplus.at

Received: 29 November 2019; Accepted: 16 April 2020

Abstract: In the current study poly(lactic acid) PLA composites with a 3 wt% and 5 wt% of nanofibrillated cellulose (NFC) were produced by 3D-printing method. An enzymatic pretreatment coupled with mechanical fibrillation in a twin screw extruder was used to produce high consistency NFC. Scanning electron microscopy (SEM) equipped with Fibermetric software, FASEP fiber length distribution analysis, Fourier transform infrared spectroscopy (FT-IR), thermogravimetric analysis (TGA), tensile tests, impact tests and differential scanning calorimetry were used to characterize NFC and PLA/NFC composites. The results of the fiber length and width measurements together with the results of the SEM analysis showed that enzymatic hydrolysis coupled with a twin screw extrusion could effectively reduce the diameter and length of cellulose fibers. The produced NFC consisted of micro- and nanosized fibers entangled in a characteristic 3D-network. Based on the FT-IR analysis, no new bonds were formed during the enzymatic hydrolysis or fibrillation process. The TGA analysis confirmed that produced NFC can be used in high-temperature extrusion processing without NFC degradation. During the PLA/NFC composites preparation the NFC agglomerates were formed, which negatively influenced PLA/NFC composites impact properties. The slightly improved tensile strength and elastic modulus were reported for all composites when compared to the neat PLA. The elongation at break was not affected by the NFC addition. No significant differences in thermal stability were detectable among composites nor in comparison with the neat PLA. However, the crystallinity degree of the composite containing 5 wt% NFC was increased in respect to the neat PLA.

Keywords: Nanofibrillated cellulose; enzymatic hydrolysis; twin screw extruder; poly (lactic acid); 3D-printing

1 Introduction

The most common processing method towards NFC isolation is mechanical fibrillation in high pressure homogenizers, microfluidizers or grinders. The main drawback related to homogenizers and microfluidizers, after high energy consumption is the clogging problem, because of its very small orifice size. The final product is a low consistency NFC suspension (1 wt%–2 wt%) which causes additional transport, storage and drying costs [1]. Therefore, the development of the new, energy efficient and environmentally



This work is licensed under a Creative Commons Attribution 4.0 International License, which permits unrestricted use, distribution, and reproduction in any medium, provided the original work is properly cited.

friendly disintegration methods becomes a priority in the industrialization of NFC. The possibility of the NFC production at the high solid content by means of a twin screw extruder (TSE) represents a great interest for industry production. The effect of the fibrillation process through a TSE on properties of never dried bleached sulfite pulp has been studied. The degree of fibrillation was enhanced with higher number of passes, but after 14 passes the temperature exceeded 40°C and degradation occurred. The output of the fibrillated fibers had a solid content up to 50 wt% [2]. In our previous study [3], the NFC at a high solid content was produced by means of a TSE. Thermogravimetric analysis showed no degradation during repeated fibrillation in a TSE and the resulting NFC was a mixture of micro- and nanofibers entangled in a dense network. However, even after 20 passes through the TSE, some microfibers and fiber bundles were present. In order to facilitate mechanical fibrillation to obtain the uniform size of the final product the use of pretreatments has been reported. The pretreatment type strongly influences the resulting NFC quality and properties, but also industrialization possibilities [1]. It was reported that NFC produced from enzymatically pretreated cellulosic wood fibers showed more favorable structure than nanofibers subjected to acid hydrolysis. Also, higher average molar mass and larger aspect ratios were found when enzymatic treatment was used [4]. In another study [5], enzymatic pretreatment followed by mechanical grinding was used to produce length controlled NFC. Pure grinding resulted in an inhomogeneous distribution of the fibers while enzymatically treated cellulose pulp showed uniformed structures. Recently, production of NFC by using enzymatic pretreatment followed by seven passes through the TSE has been reported. The resulting NFC had nanometric size, good mechanical properties and transparency. The energy demand for fibrillation was lower compared to the energy used by a grinder for the same pulp [6].

Biodegradable polymers such as PLA are gaining a lot of attention as an alternative to petroleum based products. PLA is thermoplastic aliphatic polyester derived from renewable resources, and has high strength, good optical transparency and a high modulus, when compared to other synthetic polymers. However, it has several drawbacks such as brittleness, low thermal stability and low crystallization ability [7]. One way to overcome these drawbacks without affecting the biodegradability of the polymer is use of reinforcements from biological origin. NFC is a promising additive for PLA due to its interesting properties and sustainability. Generally, the incorporation of NFC into the PLA matrix results in composites with biodegradable properties, enhanced crystallization, and improved mechanical and thermal properties, compared to the neat PLA matrix [8]. Homogeneous dispersion and interfacial adhesion of the hydrophilic NFC within the PLA matrix are the major challenges in PLA/NFC composites preparation. To address these challenges various processing methods have been investigated, e.g., solvent casting [9,10], master batch [11], and melt compounding [12,13]. Because of its biodegradability and renewability, PLA/natural fiber composites can be used in the packaging industry, agriculture, electronics, medical applications and the automotive industry [14]. Moreover, PLA is one of the few plastics suitable for 3D-printing, a very interesting technology which enables efficient use of raw materials with minimal waste, accurate control of the complex structures, design optimization and customization [15].

In this study, the high consistency NFC was produced by mechanical fibrillation of never dried cellulose pulp in a TSE. The enzymatic pretreatment was used to facilitate the fibrillation process. The obtained NFC was further used to reinforce PLA filaments for 3D-printing. The effect of NFC content (3 wt% and 5 wt%) on mechanical and thermal properties of the composites was evaluated. The SEM analysis, Fibermetric software, FASEP fiber length distribution analysis, FT-IR analysis, TGA, differential scanning calorimetry (DSC) and mechanical tests were used to characterize NFC and PLA/NFC composites.

2 Materials and Methods

2.1 Materials

The commercial spruce cellulose pulp (AustroCel Hallein GmbH, Hallein, Austria) has been provided in never-dried form and used as the raw material. The enzyme used was Celluclast 1.5 L (Novozymes,

Copenhagen, Denmark), a mixture of endoglucanase and exoglucanase with the declared activity of 700 EGU/g. Chloroform used as a biocide was purchased from Carl Roth GmbH. Acetic acid and sodium acetate used for buffer preparation were purchased from Sigma Aldrich. The PLA produced by Nature Works LLC (Blair, Nebraska, USA) under the trade name Ingeo 3251D with MFR 210°C/2.16 kg = 80 g 10 min⁻¹ was used as a polymer matrix.

2.2 Enzymatic Pretreatment

The cellulose pulp was soaked in distilled water and left to swell for 24 h in order to make cellulose more accessible for enzymatic hydrolysis. The 10-liter Nutsch filter glass reactor (Büchi AG, Switzerland) was loaded with distilled water, heated to 50°C and the cellulose pulp to a total concentration of 3 wt% was added. The pH was adjusted to 5 and the enzyme was added to start the hydrolysis (10.5 EGU/g related to the pulp weight). The reaction was carried out under stirring (400 rpm for the first hour and then reduced to 200 rpm) for 2 hours. The suspension was filtered; the reactor was loaded with fresh distilled water and incubated again at 80°C for 15 minutes to stop the enzymatic activity, then filtered and washed again. The 0.01 wt% chloroform was used as a biocide. The dry content was adjusted to 30 wt% and the cellulose pulp was stored in a freezer until use for mechanical fibrillation. The enzymatically pretreated cellulose pulp was further denoted as E-Cellulose pulp.

2.3 Mechanical Fibrillation by TSE

The E-Cellulose pulp with a solid content of about 30 wt% was mechanically fibrillated using a TSE (Brabender GmbH, Duisburg, Germany) with an L/D ratio of 40. The screw design and process parameters were chosen according to our previous study [3]. The screw design was a combination of feeding, kneading and mixing elements designed to effectively fibrillate the pulp while preserving the length of the fibers. The processing temperature was set to 25°C to avoid excessive drying of the E-Cellulose pulp, the screw speed was 400 rpm and total output was 5 kg/h. The total number of passes through the TSE was 10, and the produced NFC was further denoted as E-NFC10.

2.4 Preparation of PLA/E-NFC Composites

The neat PLA and E-NFC10 were melt compounded using a lab scale TSE (Brabender GmbH, Duisburg, Germany), with an L/D of 40. The materials were fed gravimetrically using a side feeder for E-NFC10 and a main feeder for PLA feeding. The screw speed was set at 350 rpm and the compound output was approximately 8 kg/h. The TSE set-up and temperature profile used in the compounding of PLA/NFC composites is shown in Fig. 1a. For pelletizing, the Econ Underwater Pelletizing System EUP50 (Weisskirchen, Austria) was used. All materials were dried in an oven set to 80°C for 3 h prior to filament extrusion. The filaments were prepared using a TSE (Brabender GmbH, Duisburg, Germany) with optimized 1.8 mm die. The screw speed was set to 25 rpm, the total output was 27 cm³/min, and the temperature profile is shown in Fig. 1b. The filament diameter was controlled with BETA LaserMike AccuScan 5012 (Dayton, Ohio). A filament winder system AMH 250-80 (Hubral Maschinenbau, Pfungstadt, Germany) was used to collect the extruded filaments.

From the obtained filaments, shouldered test bar specimens were printed using the German RepRap X400 3D printer (Feldkirchen, Germany). The printing nozzle with a diameter of 0.8 mm was used. The layer height was 0.3 mm and the print speed was 30 mm/s at a temperature of 220°C. In order to obtain control sample, the neat PLA sample was manufactured in the same method as composite material, without adding E-NFC10, and it was labeled as PLAref. Additionally, the “as received” PLA pellets were printed without previous thermal processing and denoted as PLA. Schematic illustration of the composite preparation methods is shown in Fig. 2 and an overview of the used PLA/E-NFC10 composites and their formulations is presented in Tab. 1. All specimens were conditioned in a climate cabinet at 23°C and 50% relative humidity for at least five days before mechanical testing.

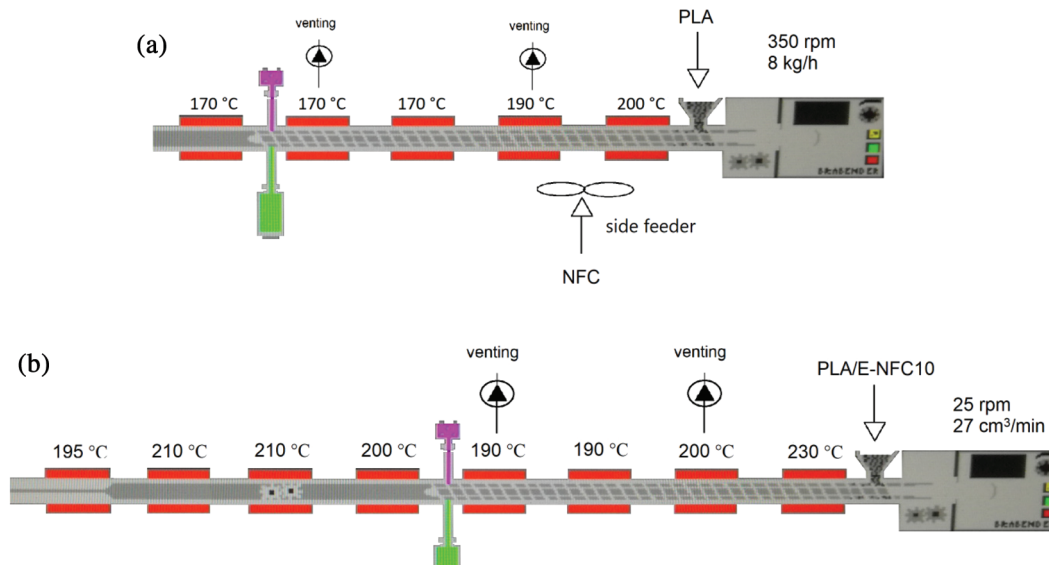


Figure 1: The TSE set-up and temperature profile used in the compounding (a) and filament extrusion (b) of the PLA and PLA/E-NFC10 composites

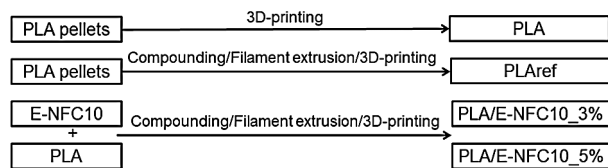


Figure 2: Schematic illustration of the composites preparation

Table 1: List of PLA/E-NFC10 composites code names and formulations

Code	PLA [%]	E-NFC10 [%]	Process
PLA	100	0	3D-printing
PLAref	100	0	Melt compounding Filament extrusion 3D-printing
PLA/E-NFC10_3%	97	3	Melt compounding Filament extrusion 3D-printing
PLA/E-NFC10_5%	95	5	Melt compounding Filament extrusion 3D-printing

2.5 Characterization Methods

2.5.1 Fiber Width and Length Distribution

Fiber width analysis was performed for cellulose pulp before and after enzymatic pretreatment on 100 single fibers selected using Fibermetric software. For each sample, 10 SEM images on 10 different spots were taken and 10 randomly chosen fibers were measured per image.

To determine the length of cellulose fibers before and after pretreatment, the 3E-ECO FASEP system (IDM Systems, Darmstadt, Germany) was used. About 5 mg of cellulose fibers was suspended in 80 ml ethanol and intensively shaken to achieve fiber separation. The representative part of the suspension was transferred into a Petri dish and analyzed.

2.5.2 SEM

The morphology of the cellulose pulp before and after pretreatment and fibrillation was observed under a Phenom Pro X SEM (Phenom-World, Eindhoven, Netherlands) with an acceleration voltage of 15 kV. A drop of a 0.1 wt% fiber aqueous suspension was deposited on a carbon-coated grid, air dried and sputter coated with gold in a SC7620 mini sputter coater (Quorum Technologies Ltd., Kent, UK).

The morphology of the neat PLA and PLA/E-NFC10 composites was observed by a Phenom ProX SEM with 15 kV accelerating voltage. The notched samples used during Charpy impact strength testing were sputter coated with gold and viewed perpendicularly to the fracture surface.

2.5.3 FT-IR

The FT-IR spectra were recorded in transmission mode via FT-IR Vertex 70 spectrometer (Bruker Optik GmbH, Ettlingen, Germany) fitted with an attenuated total reflection (ATR) detector. The infrared spectra were recorded between 4000 cm^{-1} and 400 cm^{-1} for fibers and between 4000 cm^{-1} and 600 cm^{-1} for composites, at a resolution of 4 cm^{-1} . A clean, empty diamond crystal was used for the collection of the background spectrum.

2.5.4 TGA

The thermal stability of the fibers and composites was analyzed using a Perkin Elmer TGA 4000 (PerkinElmer Inc, Waltham, USA), operated from 30°C to 600°C at 10 °C/min in dry nitrogen gas atmosphere.

2.5.5 Mechanical Tests

Tensile properties were tested according to ISO 527 using a Beta 20/10 4 × 11 universal testing machine (Messphysik GmbH, Fürstenfeld, Austria). The result is the average of six samples. Charpy notched (NIS) and unnotched (IS) impact strength was determined following ISO 179 using an Instron CEAST 90/50 impact tester (ITW Test and measurement Italia S.r.l, Torino, Italy). Ten specimens each were measured notched and unnotched at room temperature.

2.5.6 DSC

The crystallinity of the neat PLA and PLA/E-NFC10 composites was determined using a DSC (DSC 200, TA instruments, Delaware, USA). A 10 mg sample was heated from 25°C to 195°C at a heating rate of 10°C/min, then cooled and reheated at the same heating rate as before. Three measurements were performed for each material to ensure statistical validity. The data were acquired from the second heating scan. The crystallinity degree (X_c) was calculated according to Eq. (1):

$$X_c = \left[\frac{\Delta H_m - \Delta H_c}{f \times \Delta H_m^0} \right] \times 100\% \quad (1)$$

where ΔH_m is the melting enthalpy, ΔH_c is the cold crystallization enthalpy, ΔH_m^0 is the melting enthalpy for pure crystalline PLA (93 J/g), and f is the weight fraction of PLA in the nanocomposite [16].

3 Results and Discussion

3.1 Fiber Morphology and Structure

The cellulose pulp had a width between 15 μm and 60 μm with most of the fibers having a width between 21 μm and 24 μm , as shown in Fig. 3a. After enzymatic pretreatment, the fiber width was

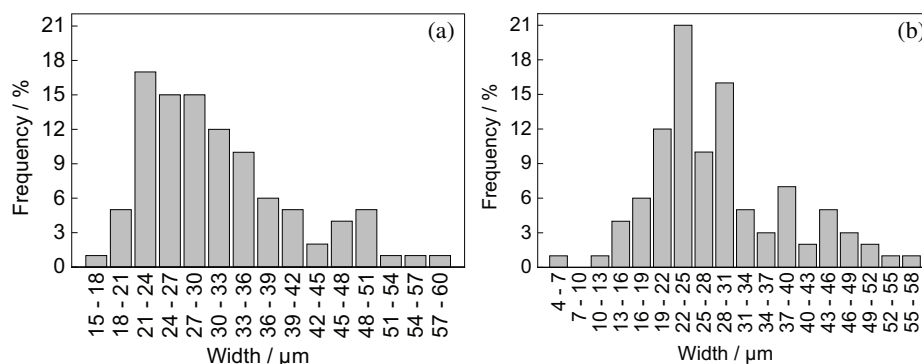


Figure 3: Width distribution of the cellulose pulp (a) and E-Cellulose pulp (b)

slightly reduced and most of the fibers had a width between 22 μm and 25 μm (Fig. 3b). However, fiber length was strongly affected by the enzymatic pretreatment. The results of the fiber length analysis with corresponding optical micrographs as insets are presented in Fig. 4. The weight average length of the cellulose pulp was 888.3 μm, and after enzymatic pretreatment the weight average length of the cellulose pulp reduced to 485.3 μm.

These data are in agreement with the observations from SEM analysis shown in Fig. 5. The cellulose pulp had a compact fiber structure. After enzymatic hydrolysis, the fiber length was reduced, the surface of the fibers was disrupted, and the microfibrils still partially connected to each other, could be visualized. Multiple fibrillations in a TSE resulted in a further separation of the fibers, and the final product was a highly entangled network of micro and nanofibers with a 30 wt% dry content. Compared to the low consistency NFC suspensions produced by conventional methods (2 wt%), the extruded NFC showed similar morphology with much higher consistency. During the fibrillation process, the processing temperature was set to 25°C to avoid excessive drying of the pulp. Contrary to our previous study [3], where processing temperature increased up to 50°C during fibrillation of the non-pretreated cellulose pulp, the processing temperature was almost constant during E-Cellulose pulp fibrillation (25°C–28°C).

The FTIR analysis was used to indicate possible changes to the molecular structure of the pulp after enzyme pretreatment and mechanical fibrillation. FT-IR spectra of the cellulose pulp, E-Cellulose pulp and E-NFC10 are presented in Fig. 6. In the FT-IR spectrum of the cellulose pulp, the absorption peak at 3315 cm⁻¹ is attributed to stretching of O–H groups, and the peak at 2901 cm⁻¹ is due to stretching of the C–H groups [17]. The absorption peak at 1673 cm⁻¹ was reported as the O–H vibration of absorbed water [17,18]. The peak for C–H and C–O vibrations contained in the polysaccharide rings of cellulose is around 1326 cm⁻¹. The absorption peak at 1033 cm⁻¹ indicates C–O– stretching vibration in glucose ring [19]. No difference was found between the spectra of E-Cellulose pulp or E-NFC10 and cellulose pulp. This result suggests that there are no new bonds formed during the enzymatic hydrolysis and mechanical fibrillation.

The thermostability of NFC is an important parameter that influences its potential application in composites. The TGA analysis was used to examine the possible changes in thermal stability of the NFC caused by the enzymatic pretreatment or mechanical fibrillation. The TG and DTG curves are shown in Figs. 7a and 7b. All curves appeared to follow similar degradation mechanism with two main weight losses. The first weight loss observed in the range from 30°C to 100°C is attributed to the evaporation of water [20]. The degradation of cellulose pulp starts at a temperature of 335.7°C and the maximum degradation temperature was observed at 380.4°C. The enzymatic pretreatment followed by mechanical fibrillation did not cause any significant changes in thermal stability. The E-Cellulose pulp degrades in the range from 332.1°C–377.8°C, while the onset temperature for thermal degradation and maximum

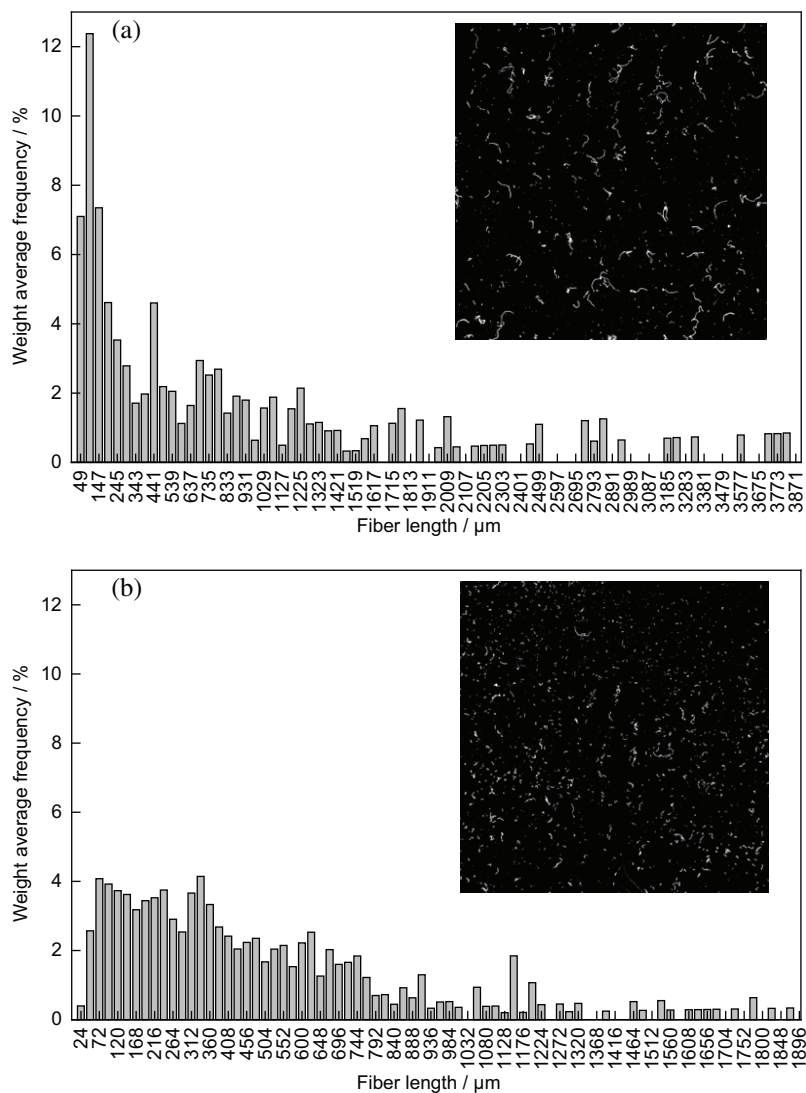


Figure 4: Length distribution of the cellulose pulp (a) and E-Cellulose pulp (b)

degradation temperature of the E-NFC10 were 336°C and 380.5°C, respectively. The mass residues of 7.76%, 4.01% and 3.46% were measured for cellulose pulp, E-Cellulose pulp and E-NFC10, respectively.

3.2 Composites Morphology, Mechanical and Thermal Properties

To provide information about the distribution of the E-NFC10 in the PLA matrix, SEM analysis was performed. As shown in Fig. 8, the neat PLA and PLAref showed a smooth fracture surface with characteristic voids that occur at the intersection of consecutive 3D-printed layers [21]. Incorporation of the E-NFC10 into the PLA matrix led to an E-NFC10 agglomeration in all composites. Moreover, the poor interaction/adhesion between the E-NFC10 and the PLA matrix was observed.

In order to investigate the phase behavior of the composites, the FT-IR experiments were performed and the results are shown in Fig. 9. The peaks at 2998 cm^{-1} and 2935 cm^{-1} are assigned to the asymmetric and symmetric C-H stretching, respectively. The C=O stretching band appears at 1747 cm^{-1} , the asymmetric bending absorption of CH_3 appears at 1450 cm^{-1} , and the peaks at 1380 cm^{-1} and 1356 cm^{-1} are

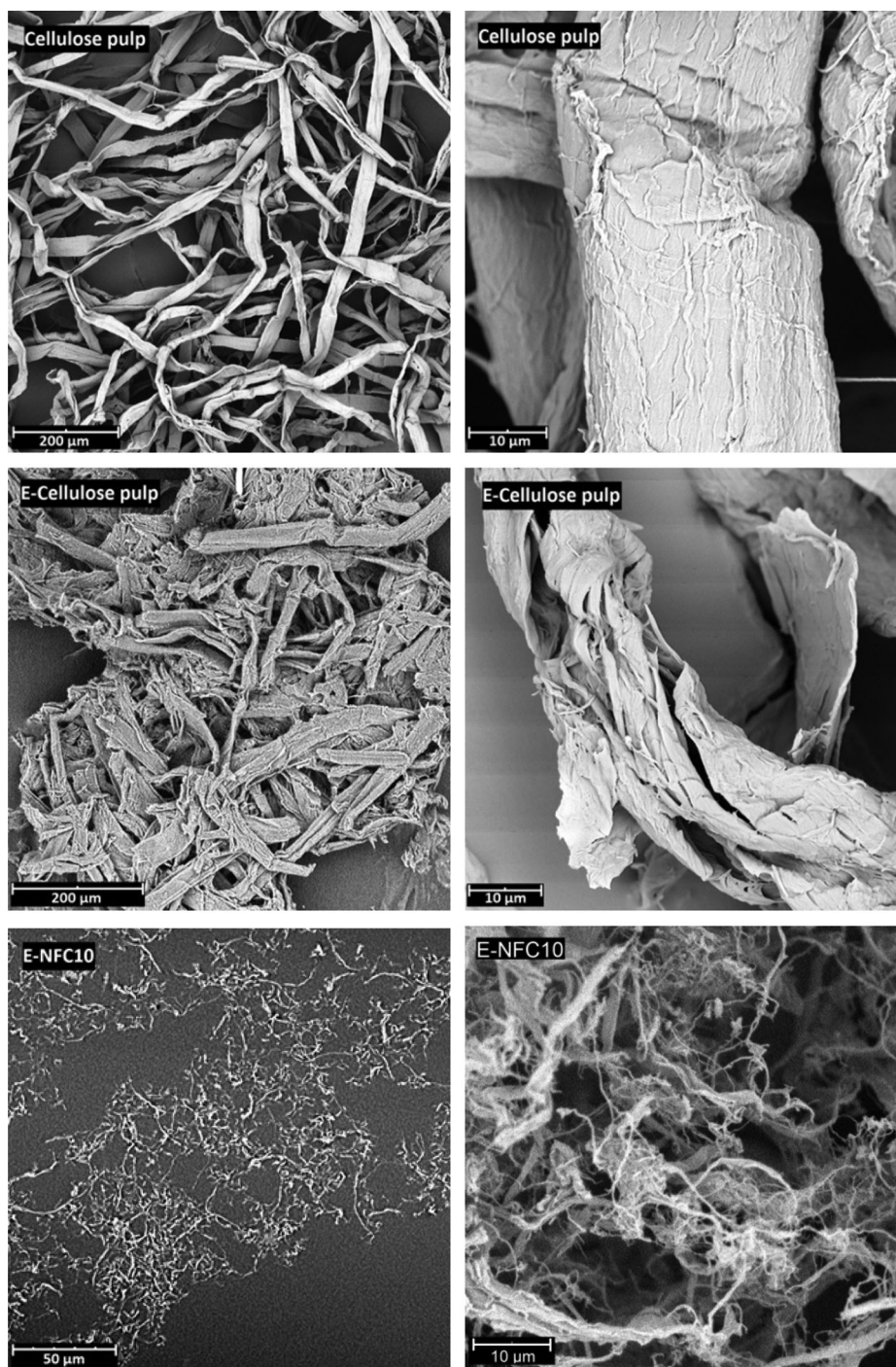


Figure 5: SEM images of the cellulose pulp, E-Cellulose pulp and E-NFC10

assigned as the symmetric bending absorption of CH_3 [22,23]. The stretching absorption of C–O–C have been identified at the 1180 cm^{-1} and 1080 cm^{-1} [24]. The two peaks at 867 cm^{-1} and 756 cm^{-1} can be attributed to the amorphous and crystalline phases of the PLA, respectively [25]. As can be seen from the Fig. 9, the spectrum of PLA and PLAref coincided with the spectra of PLA/E-NFC10 composites, proving that addition of E-NFC10 did not cause chemical changes of the biopolymer. The FT-IR spectra

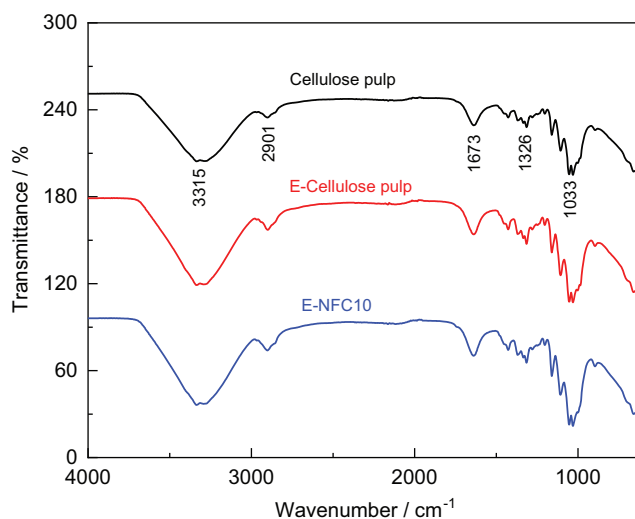


Figure 6: FT-IR spectra of cellulose pulp and E-Cellulose pulp before and after mechanical fibrillation

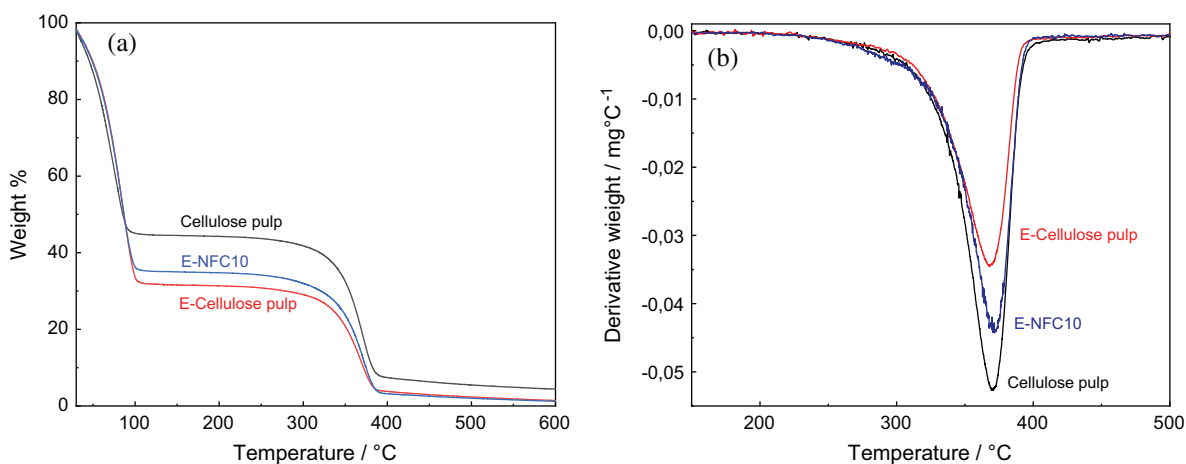


Figure 7: TG curves (a) and DTG curves (b) of cellulose pulp, E-Cellulose pulp and E-NFC10

of the neat PLA and the PLA/E-NFC10 composites did not show any evidence of interfacial interaction between the polymer and the fibers.

Mechanical properties of the 3D-printed neat PLA and the PLA/E-NFC10 composites are summarized in [Tab. 2](#). For neat PLAref, a tensile strength of 28.75 MPa was measured, and addition of 3 wt% and 5 wt% increased the tensile strength to 35.44 MPa and 32.55 MPa, respectively. A slight increase in elastic modulus was observed in all samples when compared to the PLAref ([Fig. 10a](#)). No significant changes in elongation at break were observed. As shown in [Fig. 10b](#), addition of E-NFC10 to the PLA matrix led to a slight decrease in both, notched and unnotched impact strength of the composites.

The thermal stability of the neat PLA and PLA/E-NFC10 composites was evaluated by TGA, and the results are shown in [Fig. 11](#). The decomposition of the PLAref starts at 364.4°C, and the maximum degradation temperature was 405.2°C. The presence of E-NFC10 did not have any noticeable effect on the composite's thermal stability. The onset temperatures for thermal degradation of the composites with 3 wt% and 5 wt% were 361.6°C and 360.5°C, and the maximum degradation temperatures of 402.5°C and 404.6°C were measured. The mass residues of 0.96%, 0.99%, 1.04% and 1.22% were measured for

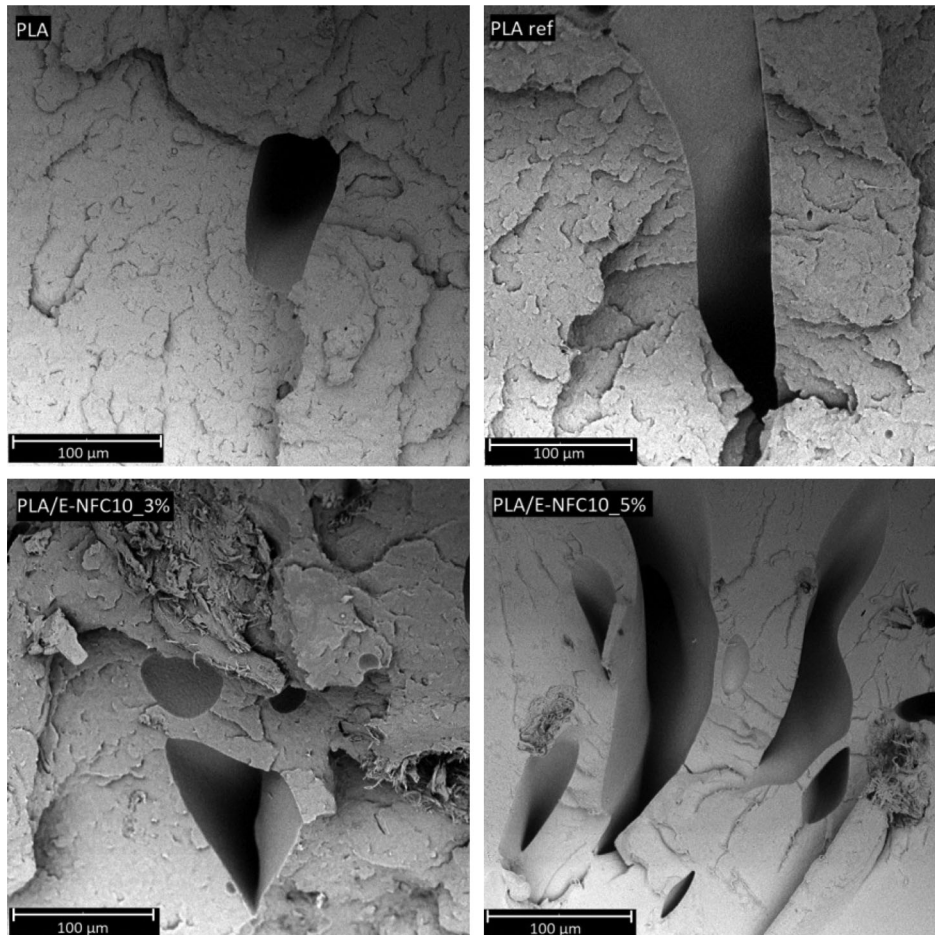


Figure 8: SEM images of the PLA and PLA/E-NFC10 composites

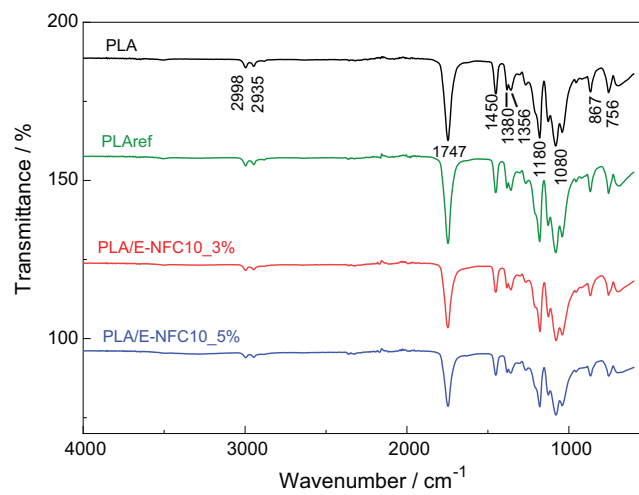
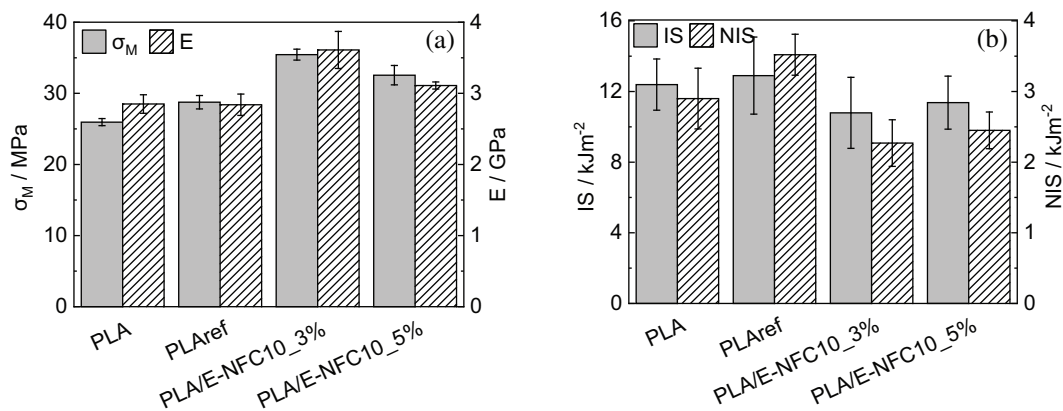
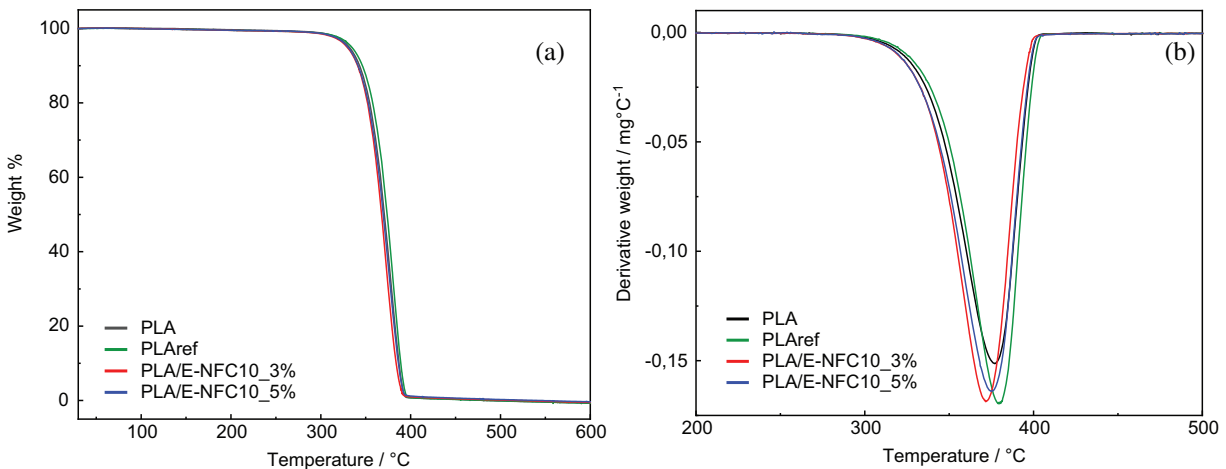


Figure 9: FT-IR spectra of the PLA and the PLA/E-NFC10 composites

Table 2: Mechanical properties of the 3D-printed neat PLA and the PLA/E-NFC10 composites

Sample	E [GPa]	σ_M [MPa]	ε_B [%]	IS [kJ/m ²]	NIS [kJ/m ²]
PLA	2.85 ± 0.13	25.95 ± 0.50	1.26 ± 0.05	12.39 ± 1.45	2.90 ± 0.43
PLAref	2.84 ± 0.15	28.75 ± 0.94	1.24 ± 0.05	12.90 ± 2.18	3.52 ± 0.29
PLA/E-NFC10_3%	3.61 ± 0.26	35.44 ± 0.77	1.23 ± 0.05	10.79 ± 2.01	2.27 ± 0.33
PLA/E-NFC10_5%	3.11 ± 0.05	32.55 ± 1.36	1.26 ± 0.05	11.37 ± 1.50	2.45 ± 0.26

**Figure 10:** Tensile properties (a) and impact properties (b) of the PLA and PLA/E-NFC10 composites**Figure 11:** TG curves (a) and DTG curves (b) of the neat PLA and PLA/E-NFC10 composites

PLA, PLAref, PLA/E-NFC10_3% and PLA/E-NFC10_5%, respectively. The enhancement of the thermal stability of the nanocomposite is strongly dependent on the level of dispersion and the final morphology of the nanocomposites [26]. The lack of improvement in thermal stability could be ascribed to the E-NFC10 inhomogeneous dispersion, agglomeration and poor interfacial adhesion in PLA matrix.

The glass transition temperature (T_g), cold crystallization (T_{cc}) and melting transition (T_m) of the PLA and PLA/E-NFC10 composites were studied by DSC. The second heating scan is shown in Fig. 12. Thermal transitions and degree of crystallinity (X_c) of the materials are summarized in Tab. 3. The PLAref showed

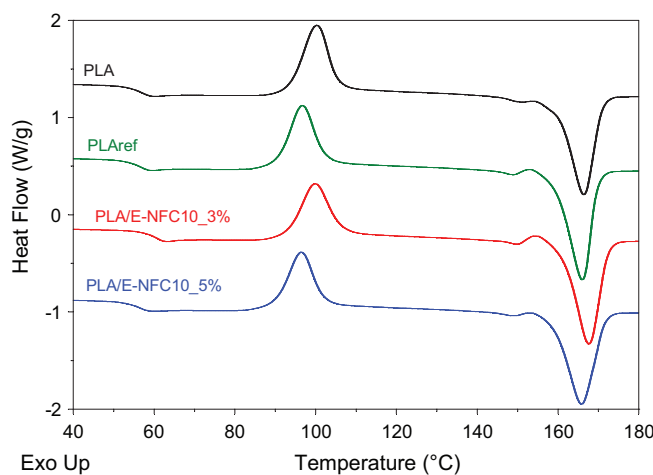


Figure 12: Second heating scan of the PLA and PLA/E-NFC10 composites

Table 3: Thermal properties of the 3D-printed neat PLA and PLA/E-NFC10 composites calculated from the second heating scan

Sample	T_g [°C]	T_{cc} [°C]	T_m [°C]	X_c [%]
PLA	59.8	102.8	167.7	10.93
PLAref	60.0	99.7	167.6	11.81
PLA/E-NFC10_3%	61.2	100.8	168.0	12.54
PLA/E-NFC10_5%	57.9	97.5	166.5	14.22

T_g at 60°C, followed by cold crystallization peak at 99.7°C and a melting peak at 167.6°C. The addition of 5 wt% E-NFC10 slightly decreased the T_g of the composites and shifted the T_{cc} to lower temperatures when compared to the PLAref. Right before the melting peak, the small shoulder peak was observed for PLAref and PLA/E-NFC10 composites. According to literature [27], the appearance of the shoulder peak is possibly associated with the phase transition from α' -crystal form with loose and disordered chain packing to an ordered α -crystal form during the heating. When 5 wt% E-NFC10 was added to the PLAref, the shoulder peak was smaller when compared to PLAref, which suggests that addition E-NFC10 likely supports the formation of more stable α -crystal form of the PLA. No significant changes in T_m could be observed when E-NFC10 was added to the PLA matrix. A slightly higher X_c was obtained for PLA/E-NFC10_5% composite (14.22%) with respect to the PLAref (11.81%).

4 Conclusion

The goal of this research was to improve the mechanical properties of the PLA by using high consistency NFC as a reinforcing. The high consistency NFC was successfully produced by using enzymatic pretreatment followed by mechanical fibrillation in a TSE.

The morphology study revealed characteristic highly entangled 3D-network of micro- and nanofibers. Based on the FT-IR analysis, no new bonds were formed during the enzymatic hydrolysis or fibrillation process. The thermal stability of the fibers was not affected by enzymatic pretreatment nor mechanical fibrillation.

PLA/NFC composites were prepared through melt mixing of PLA with 3 wt% and 5 wt% of E-NFC10 using twin screw extrusion. After mixing in a TSE, the filaments for 3D-printing were produced, and specimens for tensile and impact strength test were printed.

The tensile strength of the PLA increased from 28.75 MPa in PLAREf to 35.44 MPa and 32.55 MPa with the addition of 3 wt% E-NFC10 and 5% E-NFC10, respectively. A slight increase in elastic modulus for all composites was also observed when compared to the PLAREf. The greatest impact is related to the sample that contains 3 wt% E-NFC10, which showed 27.11% increase in elastic modulus, compared to the PLAREf. The incorporation of E-NFC10 had no impact on the elongation at break.

The morphology studies of PLA and its nanocomposites revealed E-NFC10 aggregates in the fracture surfaces of the PLA/E-NFC10_3% and PLA-PLA/ENFC10_5% composites. Due to the agglomeration of E-NFC10, the impact strength of the PLA/E-NFC10 composites was slightly decreased when compared to the neat PLAREf.

The thermal stability was not affected by the E-NFC10 incorporation. However, the addition of 5 wt% E-NFC10 slightly increased composites crystallinity.

Acknowledgement: This work was conducted within the scope of the INTERREG Österreich—Bayern 2014–2020 project.

Funding Statement: The author(s) received no specific funding for this study.

Conflicts of Interest: The authors declare that they have no conflicts of interest to report regarding the present study.

References

1. Kargarzadeh, H., Ioelovich, M., Ahmad, I., Thomas, S., Dufresne, A. (2017). Methods for extraction of nanocellulose from various sources. In: Kargarzadeh, H., Ahmad, I., Thomas, S., Dufresne, A. (eds.) *Handbook of Nanocellulose and Cellulose Nanocomposites*. Vol. 1. pp. 1–51. Weinheim, Germany: Wiley-VCH.
2. Ho, T. T. T., Abe, K., Zimmermann, T., Yano, H. (2015). Nanofibrillation of pulp fibers by twin-screw extrusion. *Cellulose*, 22(1), 421–433. DOI 10.1007/s10570-014-0518-6.
3. Perić, M., Putz, R., Paulik, C. (2019). Influence of nanofibrillated cellulose on the mechanical and thermal properties of poly (lactic acid). *European Polymer Journal*, 114, 426–433. DOI 10.1016/j.eurpolymj.2019.03.014.
4. Henriksson, M., Henriksson, G., Berglund, L. A., Lindström, T. (2007). An environmentally friendly method for enzyme-assisted preparation of microfibrillated cellulose (MFC) nanofibers. *European Polymer Journal*, 43(8), 3434–3441. DOI 10.1016/j.eurpolymj.2007.05.038.
5. Chen, Y., Fan, D., Han, Y., Li, G., Wang, S. (2017). Length-controlled cellulose nanofibrils produced using enzyme pretreatment and grinding. *Cellulose*, 24(12), 5431–5442. DOI 10.1007/s10570-017-1499-z.
6. Rol, F., Karakashov, B., Nechyporchuk, O., Terrien, M., Meyer, V. et al. (2017). Pilot-scale twin screw extrusion and chemical pretreatment as an energy-efficient method for the production of nanofibrillated cellulose at high solid content. *ACS Sustainable Chemistry & Engineering*, 5(8), 6524–6531. DOI 10.1021/acssuschemeng.7b00630.
7. Sin, L. T., Rahmat, A. R., Rahman, W. A. W. A. (2012). *Poly(lactic acid): PLA biopolymer technology and applications*. Oxford: William Andrew.
8. Ding, W. D., Pervaiz, M., Sain, M. (2018). Cellulose-enabled poly(lactic acid) (PLA) nanocomposites: recent developments and emerging trends. In: Thakur, V. K., Thakur, M. K. (eds.) *Functional Biopolymers*. pp. 183–216. Cham: Springer.
9. Iwatake, A., Nogi, M., Yano, H. (2008). Cellulose nanofiber-reinforced poly(lactic acid). *Composites Science and Technology*, 68(9), 2103–2106. DOI 10.1016/j.compscitech.2008.03.006.
10. Suryanegara, L., Nakagaito, A. N., Yano, H. (2009). The effect of crystallization of PLA on the thermal and mechanical properties of microfibrillated cellulose-reinforced PLA composites. *Composites Science and Technology*, 69(7–8), 1187–1192. DOI 10.1016/j.compscitech.2009.02.022.

11. Jonoobi, M., Harun, J., Mathew, A. P., Oksman, K. (2010). Mechanical properties of cellulose nanofiber (CNF) reinforced polylactic acid (PLA) prepared by twin screw extrusion. *Composites Science and Technology*, 70 (12), 1742–1747. DOI 10.1016/j.compscitech.2010.07.005.
12. Mathew, A. P., Oksman, K., Sain, M. (2005). Mechanical properties of biodegradable composites from poly lactic acid (PLA) and microcrystalline cellulose (MCC). *Journal of Applied Polymer Science*, 97(5), 2014–2025. DOI 10.1002/app.21779.
13. Oksman, K., Mathew, A. P., Bondeson, D., Kvien, I. (2006). Manufacturing process of cellulose whiskers/polylactic acid nanocomposites. *Composites Science and Technology*, 66(15), 2776–2784. DOI 10.1016/j.compscitech.2006.03.002.
14. Fiori, S. (2014). Industrial uses of PLA. In: Jiménez, A., Peltzer, M., Ruseckaite, R. (eds.) *Poly (lactic acid) Science and Technology*. pp. 315–333. Cambridge: Royal Society of Chemistry.
15. Huang, S. H., Liu, P., Mokasdar, A., Hou, L. (2013). Additive manufacturing and its societal impact: a literature review. *International Journal of Advanced Manufacturing Technology*, 67(5-8), 1191–1203. DOI 10.1007/s00170-012-4558-5.
16. Song, Y., Tashiro, K., Xu, D., Liu, J., Bin, Y. (2013). Crystallization behavior of Poly (lactic acid)/microfibrillated cellulose composite. *Polymer*, 54(13), 3417–3425. DOI 10.1016/j.polymer.2013.04.054.
17. Wulandari, W. T., Rochliadi, A., Arcana, I. M. (2016). Nanocellulose prepared by acid hydrolysis of isolated cellulose from sugarcane bagasse. *IOP Conference Series: Materials Science and Engineering*, 107, 012045. DOI 10.1088/1757-899X/107/1/012045.
18. Hospodarova, V., Singovszka, E., Stevulova, N. (2018). Characterization of cellulosic fibers by FTIR spectroscopy for their further implementation to building materials. *American Journal of Analytical Chemistry*, 9(6), 303–310. DOI 10.4236/ajac.2018.96023.
19. Hu, J., Tian, D., Rennecker, S., Saddler, J. N. (2018). Enzyme mediated nanofibrillation of cellulose by the synergistic actions of an endoglucanase, lytic polysaccharide monoxygenase (LPMO) and xylanase. *Scientific Reports*, 8(1), 3195. DOI 10.1038/s41598-018-21016-6.
20. Sofla, M. R. K., Brown, R. J., Tsuzuki, T., Rainey, T. J. (2016). A comparison of cellulose nanocrystals and cellulose nanofibres extracted from bagasse using acid and ball milling methods. *Advances in Natural Sciences: Nanoscience and Nanotechnology*, 7(3), 035004. DOI 10.1088/2043-6262/7/3/035004.
21. Benwood, C., Anstey, A., Andrzejewski, J., Misra, M., Mohanty, A. K. (2018). Improving the impact strength and heat resistance of 3D printed models: structure, property, and processing correlations during fused deposition modeling (FDM) of poly (lactic acid). *ACS Omega*, 3(4), 4400–4411. DOI 10.1021/acsomega.8b00129.
22. Chieng, B., Ibrahim, N., Yunus, W., Hussein, M. (2014). Poly (lactic acid)/Poly (ethylene glycol) polymer nanocomposites: effects of graphene nanoplatelets. *Polymers*, 6(1), 93–104. DOI 10.3390/polym6010093.
23. Luu, P. D., Truong, H. T., van Luu, B., Pham, L. N., Imamura, K. et al. (2014). Production of biodiesel from Vietnamese *Jatropha curcas* oil by a co-solvent method. *Bioresource Technology*, 173, 309–316. DOI 10.1016/j.biortech.2014.09.114.
24. Cai, Y., Lv, J., Feng, J. (2013). Spectral characterization of four kinds of biodegradable plastics: Poly (Lactic Acid), Poly (Butylenes Adipate-Co-Terephthalate), Poly (Hydroxybutyrate-Co-Hydroxyvalerate) and Poly (Butylenes Succinate) with FTIR and Raman Spectroscopy. *Journal of Polymers and the Environment*, 21(1), 108–114. DOI 10.1007/s10924-012-0534-2.
25. Goncalves, C. M. B., Coutinho, J. A. P., Marrucho, I. M. (2010). Optical properties. In: Auras, R., Lim, L. T., Selke, S. E. M., Tsuji, H. (eds.) *Poly (lactic acid): Synthesis, Structures, Properties, Processing, and Applications*. pp. 97–111. Hoboken, NJ: Wiley.
26. Gan, P. G., Sam, S. T., Abdullah, M. F., Omar, M. F. (2019). Thermal properties of nanocellulose-reinforced composites: a review. *Journal of Applied Polymer Science*, 137(11), 48544. DOI 10.1002/app.48544.
27. Zhang, J., Tashiro, K., Tsuji, H., Domb, A. J. (2008). Disorder-to-order phase transition and multiple melting behavior of poly (l-lactide) investigated by simultaneous measurements of WAXD and DSC. *Macromolecules*, 41(4), 1352–1357. DOI 10.1021/ma0706071.